# Modeling the use of transient ligand binding information by AMPA receptors

Check for updates

Helena Braunstein[1,2], Alejandra C. Ventura[1,3,4] ✉ & Alejandro Colman-Lerner[1,2,4] ✉

Glutamate mediates fast excitatory neurotransmission through α-amino-3-hydroxy-5-methyl-4-isoxazole propionic acid (AMPA)-type glutamate receptors in the central nervous system. Although it is well known that the glutamate affinity for AMPA receptors is submicromolar, ligand-dependent currents are observed only at submillimolar glutamate concentrations, suggesting a non-equilibrium mechanism of dose-dependent signaling. Here, we developed a mathematical model that leverages published reaction rates to demonstrate that AMPA receptors operate within a pre-equilibrium sensing and signaling (PRESS) regime. By functioning before equilibrium binding, AMPARs exploit a transient dynamic range at high ligand concentrations. Our model reveals that fast desensitization is a key transition enabling this PRESS mechanism. Regulators of this desensitization, such as transmembrane AMPAR regulatory proteins TARP, germ cell-specific gene 1-like protein and cornichon homolog auxiliary proteins (CNIH2/3), thus modulate AMPAR dynamic range by modifying the time window in which these receptors may use pre-equilibrium information. We speculate that the use of PRESS by AMPARs helps restrict the postsynaptic area of action of this fast transmission. Other receptors with fast desensitization may also take advantage of PRESS to accurately control dose-dependent responses.

Cells use information about external and internal conditions, and information retrieved from their genomes, in order to make decisions that determine their future actions. To transmit that information, cells evolved systems based on protein species, operating in processes as diverse as bacterial chemotaxis, sensing and metabolism of sugars, responses to morphogen gradients, as well as for the transmission of nerve impulses.

An important feature of these systems is their dynamic range, that is, the range of input concentrations that the system can distinguish. A key determinant of the dynamic range is the affinity of the input molecule for its receptor, usually measured by its dissociation constant, $K_D$, the value of which coincides with the concentration of ligand that results in 50% receptor occupancy at binding equilibrium. Low-affinity receptors (high $K_D$) cannot detect low concentrations of ligand, whereas high-affinity ones (low $K_D$) become saturated when ligand concentrations become high. One way biological systems have evolved to overcome this limitation is to express more than one receptor with different affinities according to need[1]. In our previous work[2,3] we described a mechanism, pre-equilibrium sensing and signaling (PRESS), to control the dynamic range. Taking advantage of pre-steady state information, signaling systems that operate in a PRESS regime

expand and shift the input dynamic range, enabling cells to discriminate between ligand concentrations that are indistinguishable at steady state. PRESS is based on the fact that binding reactions reach equilibrium faster at high concentrations of binding partners (ligands and receptors, for example) than at low (Fig. 1a). As a consequence, the ligand concentration-response curve is initially right-shifted (to higher ligand concentrations), but over time it shifts to the left, until binding reaches steady state (Fig. 1b). A PRESS mechanism is enabled when the signal transduction steps downstream of the binding reaction are fast enough to occur before ligand binding reaches equilibrium. In these conditions, the response to ligand binding would effectively be taking place during the transient right-shifted concentration-response curve.

In our previous work, we showed experimentally that PRESS operates during the chemotropic mating response in S. cerevisiae. Furthermore, using simplified mathematical models, we demonstrated that this mechanism is effective in systems exhibiting negative or incoherent feedback loops, and when the activated downstream component passes through an "activation-refractory" state prior to resetting[2]. In that work, we speculated that since this topology is similar to how some neurotransmitter

[1]Instituto de Fisiología, Biología Molecular y Neurociencias (IFIBYNE) CONICET-Universidad de Buenos Aires, Facultad de Ciencias Exactas y Naturales, Buenos Aires, Argentina. [2]Departamento de Fisiología, Biología Molecular y Celular, Facultad de Ciencias Exactas y Naturales, Universidad de Buenos Aires, Buenos Aires, Argentina. [3]Departamento de Física, Facultad de Ciencias Exactas y Naturales, Universidad de Buenos Aires, Buenos Aires, Argentina. [4]These authors contributed equally: Alejandra C. Ventura, Alejandro Colman-Lerner. ✉e-mail: alejvent@fbmc.fcen.uba.ar; colman-lerner@fbmc.fcen.uba.ar

**Fig. 1 | Binding reactions reach equilibrium faster at high concentrations of binding partners.**
**a** Diagram of a simple binding reaction between a receptor (R) and a ligand (L), and a plot of the fraction of occupied receptors vs time, for different ligand concentrations and a given receptor concentration. Small circles mark the time point at which receptor occupancy reaches half of the steady-state value for a given ligand concentration.
**b** Fraction of occupied receptors vs ligand concentration. Each curve corresponds to a different time after ligand addition (from early times, light gray to steady state, black). Small circles mark the ligand concentration at which receptor occupancy is half of the steady state value at each time.
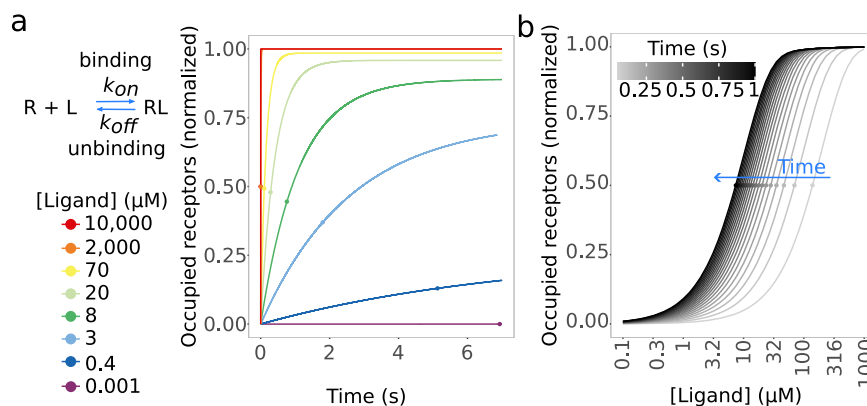


ion-channel receptors work in neurons, PRESS might be relevant to the nervous system. Here, we aim to demonstrate this.

A ubiquitous channel with the required characteristics is the central nervous system receptor of the neurotransmitter L-glutamate, the α-amino-3-hydroxy-5-methyl-4-isoxazolepropionic acid (AMPA) receptor (AMPAR), an ion channel located in excitatory synapses[4]. AMPARs mediate most fast excitatory synaptic transmission, critically governing synaptic plasticity, information processing, and network function in the brain[5]. In addition, AMPARs have a central role in synaptic function and dysfunction[6]. Despite the abundant information accumulated, a deeper understanding of their activation dynamics, particularly how they process rapid, high-concentration glutamate pulses typical of synaptic transmission, remains a challenge in contemporary neuroscience.

AMPARs are tetramers composed of any of four isoforms, GluA1-4 (also known as GluR1-4), with slightly different properties. Each AMPAR has one ligand binding site per protomer and at least two subconductances and a main conductance level, corresponding to receptors with two, three and four bound ligands, though there have been studies that describe 3 subconductance levels[7]. The events associated with AMPAR activation begin with ligand binding and are followed by a conformational change known as clamshell closure, which traps L-glutamate "inside" the ligand-binding domain, in turn followed either by the opening of the channel pore and subsequent passage of cations or by a desensitized state. The conformational changes that lead to channel opening in the AMPAR may be viewed as the first stage of the signal transduction activated by the ligand. Transduction is much faster than the speed at which glutamate dissociates from AMPAR (see below), and since the channel remains desensitized for a while, this transduction is also transient even when the input ligand is not. Thus, in principle, AMPAR meets the conditions to perform PRESS: slow binding followed by fast and transient transduction.

Here, we present a mathematical modeling-based work using published reaction rates that shows AMPARs normally operate in a PRESS regime. The model behaves much as expected, showing a much higher concentration of L-glutamate (2–3 orders of magnitude higher) required to elicit a significant current through these channels than for L-glutamate to bind the receptor[4,8]. We also present a detailed analysis of the effect of the rates of the different transitions that the channel undergoes after stimulation, highlighting the importance of the balance between rates to achieve this system-level behavior. We suggest that other receptor systems might use PRESS, provided they have sufficiently fast inactivation rates to do so.
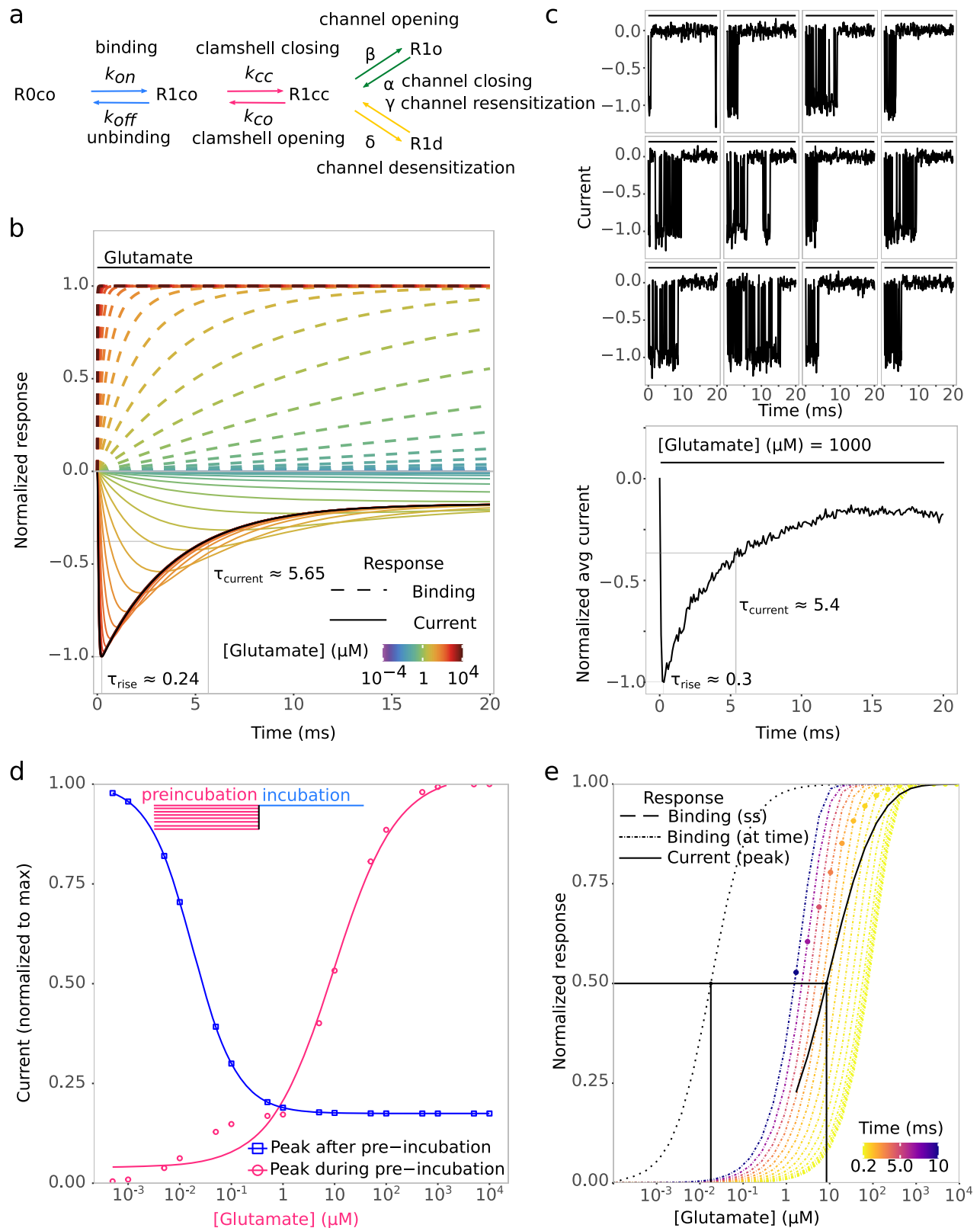
## Results

If AMPARs do in fact operate in a PRESS regime, then we expect their output dose–response to be right-shifted with respect to the L-glutamate binding reaction to AMPAR. That is, the concentration of L-glutamate required to achieve half-maximal peak current (EC$_{50}$) should be significantly higher than that required to reach half-maximal receptor occupancy at binding equilibrium (a concentration equal to the $K_D$), as we have

shown using toy models[2]. Notably, previous work has established that while the $K_D$ between L-glutamate and AMPAR is around 0.5 μM[8], the experimentally measured peak current elicited in the presence of constant L-glutamate has an EC$_{50}$ in the range of 10–200 μM, depending on the exact tetramer subunit composition[4]. That is, the output is 20–500 times less sensitive than L-glutamate binding, consistent with AMPARs using PRESS.

## A simplified model qualitatively reproduces the experimentally measured behavior

Experimental data suggested that AMPARs might, in fact, be naturally operating in PRESS mode. However, the reason for the difference between glutamate affinity for the receptor and its peak ion current EC$_{50}$, even though reproduced in earlier models, has not been not investigated explicitly. To determine if the large difference between binding $K_D$ and current EC$_{50}$ is due to PRESS, we used mathematical modeling. First, we constructed a simplified ordinary differential equations (ODEs) model, based on a previously described reaction scheme that captures the main transitions of AMPARs (Fig. 2a)[9]. In this model, AMPAR is a single subunit, which transitions reversibly through different states: **R0co** (unbound, clamshell open), **R1co** (bound, clamshell open), **R1cc** (bound, clamshell closed). **R1cc** might then open its channel into the **R1o** state or desensitize into the **R1d** state. We simulated time courses in response to step increases to various concentrations of L-glutamate (Fig. 2b) using parameters derived from the literature (Table 1, see Methods). As expected, the concentration of bound AMPAR (all species minus R0co) monotonically increased over time until it reached steady state, while the open-channel form **R1o**, representing the current passing through the channel, peaked and then declined to a low steady state over a range of ligand concentrations. At higher L-glutamate concentrations, the peak current was higher, and it was achieved earlier. The deterministic nature of an ODE model sometimes does not capture well the behavior of a collection of individual molecules, each operating in a probabilistic fashion. Thus, we also performed stochastic simulations of this simplified AMPAR model, in which each simulation represents an individual channel randomly opening and closing (Fig. 2c, top traces). Though the channels behave independently from each other, the average of many simulations of the channel resulted in a current with the same rise and desensitization times as the ODE simulation performed with the same ligand concentration (Fig. 2c, bottom). From this we concluded that the ODE model is a good approximation of a collection of channels in a synapse. In addition, a simulated pre-pulse experiment qualitatively reproduced the well-documented effect of glutamate-dependent desensitization[10] (Fig. 2d).

The binding dose–response curve (Fig. 2e) had an apparent $K_D$ of about 0.02 μM, one magnitude smaller than reported previously[8]. We suspected this difference stemmed from the fact that Abele, measured binding using the ligand binding domain of AMPAR[8], which could not open or desensitize, but our simple model could. The inclusion of these extra reactions in our model created extra species from which L-glutamate could not unbind, effectively decreasing the apparent $k_{off}$, and thereby reducing the

apparent $K_D$. Indeed, removing these extra reactions from our model resulted in an apparent $K_D$ of ~0.38 μM (Supplementary Fig. 1), a value that matches the previous measurement[8]. Importantly, the peak current dose–response curve was located far to the right of the binding curve, with an $EC_{50}$ of ~8 μM. Thus, the dynamic range of the downstream response was displaced to the high-dose region. As we have shown previously by

modeling and experiments with receptor-ligand systems, the bound state dose–response curve shifts to the left-over time[2] (Fig. 2e). Peak current at each simulated concentration of ligand occurred before the binding dose–response reached equilibrium, indicating the system's signaling is fast enough to use pre-equilibrium information, supporting the notion that in this model AMPARs use PRESS.

**Fig. 2 | A one-subunit model of AMPAR exhibits the expected qualitative behavior: a current peak followed by desensitization as ligand binding reaches a steady-state in a monotonic fashion, and a large displacement to higher concentrations of the current dose–response curve relative to steady-state binding. a** Diagram of the one-subunit model. **b** Deterministic time courses with increasing ligand concentrations. Plot shows receptor occupancy (normalized sum of all species with bound L-glutamate: R1co, R1cc, R1o, and R1d) and current (normalized species R1o, drawn with negative numbers) vs. time. Purple lines correspond to lower ligand (L-glutamate) concentration. **c** Plots show 12 single-channel current stochastic simulations with 1 mM L-glutamate (top) and the resulting average current of 500 such simulations (bottom). **d** Inset shows the design of the simulated pre-incubation experiment. Red: peak current vs L-glutamate concentration during pre-incubation. Blue: peak current obtained when stimulated with $10^4$ μM L-glutamate after being preincubated with the indicated L-glutamate concentrations. **e** The one-subunit model behavior is consistent with the channel operating in PRESS regime. Plot shows the dose–response curves for peak current (black solid), steady-state ligand binding (black dotted line), and ligand binding at different times after the addition of L-glutamate (slash-dotted lines coded using a colormap). Colored circles highlight AMPAR occupancy at the time of peak current at the indicated L-glutamate concentrations. The values used for the dose–response curves are from (**b**). Ligand concentrations that elicit 50% of maximum response are marked with solid straight black lines for the steady-state ligand binding and peak current dose–response curves. **b, c** $\tau_{current}$ and $\tau_{rise}$ correspond to the time at which peak current occurred or the time it took the current to decrease to 37% of peak current.

**Table 1 | Parameters used to model AMPAR with L-glutamate as ligand**

| Parameter | Rate | Reference |
|---|---|---|
| $k_{on}$ | 161 | 8 |
| $k_{off}$ | $1.60 \times 10^5$ | 8 |
| $k_{cc}$ | $6.30 \times 10^4$ | 8 |
| $k_{co}$ | $2.40 \times 10^1$ | 8 |
| $\alpha$ | $8.00 \times 10^3$ | 9 |
| $\beta$ | $2.00 \times 10^4$ | 9 |
| $\delta$ | 800 | 9 |
| $\gamma$ | 45 | 9 |

All rates in $s^{-1}$ except kon, in $\mu M^{-1} s^{-1}$.

Since AMPAR is a four-subunit receptor/channel, we wondered how the PRESS characteristics displayed by the one-subunit model would be altered by adding extra subunits. Thus, we constructed a four-subunit model (Figs. 3a and S2), assuming that each subunit behaved independently from the others (i.e., we used the state transition probabilities independent of binding order for all subunits, see Methods), but that the current passing through the channel depended on the number of subunits in the open state. In our model, only receptors with more than one subunit in the open conformation pass any current, receptors with three subunits in the open conformation passed twice the current as those with two, and with four subunits in the open conformation passed thrice[7]. The four-subunit model behaved qualitatively identical to the simpler version (Fig. 3b). As in that case, this model showed a smaller response when stimulated with L-glutamate after a pre-incubation with ligand (Fig. 3c), as shown experimentally[10]. Notably, in this four-subunit model, the peak current dose–response curve was located even farther to the right of the binding curve than in the one-subunit model, with an $EC_{50}$ of about 19 μM (Fig. 3d). This increased current $EC_{50}$ was a result of the conductance dependence on the number of open subunits. Since there were no qualitative differences in the behavior of this more complex model, for the rest of the paper, we used the one-subunit model.

**Enabled by a relatively slow sensing, the system operates in a pre-equilibrium regime**
In PRESS, the displacement between the input and output dose–responses is caused by the capacity of the transducing machinery to rapidly convert one into the other before binding equilibrium is reached. Thus, in this section, we modified the AMPAR model to alter the relative velocities of binding and channel operation and asked if these changes affected the relative position of the binding and current $EC_{50}$s in the expected fashion. First, we shortened the pre-equilibrium time window by increasing the four rates of the processes that precede channel opening (ligand binding/unbinding, clamshell closing/opening) by multiplying $k_{on}$, $k_{off}$, $k_{cc}$ and $k_{co}$ by a factor of 10, 100, and 1000. Indeed, as the rates got larger (faster), the simulated peak current curve shifted to the left (Fig. 4a), resulting in an $EC_{50}$ of ~0.1 μM with the

largest rates tested, radically reducing the difference between binding and current curves. In contrast, when we lengthened the pre-equilibrium time window by reducing the same rates (multiplying $k_{on}$, $k_{off}$, $k_{cc}$ and $k_{co}$ by a factor of 0.1 and 0.01), we observed the opposite effect: the current curve shifted farther to the right (Fig. 4a), increasing its $EC_{50}$ to about 5500 μM. Naturally, because we maintained the ratios of each pair of transition rates (i.e., the same binding $K_D$ and clamshell $K_{eq}$), the steady-state binding dose–response curve was not affected. Finally, because the transitions in our model are independent, changing the speed of the signal transduction steps (channel opening/closing and desensitization/resensitization) had the exact opposite effect on the dose–response curve separation (compare Fig. 4a with Supplementary Fig. 3).

We then wondered which of the four transitions of AMPAR allows the greatest separation between binding and peak current $EC_{50}$. To study that, we began by assessing the effect of changing the binding/unbinding and clamshell closing/opening rates relative to each other, maintaining fixed their respective $K_D$ and $K_{eq}$, as well as the rates for the channel opening and desensitization. We found that both for the binding and clamshell-related rates, the lower the rates, the greater the separation between the dose–response curves (Fig. 4b). Inspection of the data also revealed that the effect of binding and clamshell rates was multiplicative, suggesting their effects are independent, at least in the region of the parameter space studied. A consequence of this is that low clamshell-related rates compensated for high binding rates, and vice versa. Thus, for AMPARs, displacement of the current relative to binding $EC_{50}$ seemed to be governed by the overall speed at which the closed clamshell state, R1cc, is formed, relative to the speed of the channel transitions.

The above result was surprising, since of these two transitions of the AMPAR receptor (binding and activation), only the first one depends on ligand concentration, and as explained above, it is the ligand dependency of the dynamics that brings about the separation of the $EC_{50}$s, enabling PRESS. How is it then that the speed of the second transition affects the separation of the $K_D$ from the $EC_{50}$? To explore this question, we simulated a "truncated" model containing only these two transitions (binding and activation), for different values of $K_D$ ($k_{off}/k_{on}$) and $K_{eq}$ ($k_{co}/k_{cc}$), and calculated $\tau_{activation}$ (the time to reach 63.2% of steady-state activation), varying the binding rates (Fig. S4). We found that for systems with $K_{eq}$ equal to or greater than 1, $\tau_{activation}$'s dependency on ligand concentration depended only on binding rates, and as expected, it was lost when both $k_{on}$ and $k_{off}$ were relatively high. However, if $K_{eq}$ was lower than 1, such as in the case of the measured rates for AMPARs (clamshell closing is much faster than its opening), $\tau_{activation}$'s dependency on ligand concentration was retained even at high $k_{on}$ and $k_{off}$ values, and at higher $K_D$s. We verified that these results applied to the complete model as well, modifying the AMPARs rates so that the activation equilibrium constant was set to 1. Indeed, in this modified model, information of ligand concentration (seen as the displacement of the $EC_{50}$ of peak current relative to binding) was only dependent on binding rates (Fig. 4c).

Above, we established that speeding up the four-channel operation rates increases dose–response separation (Supplementary Fig. S3). To tease
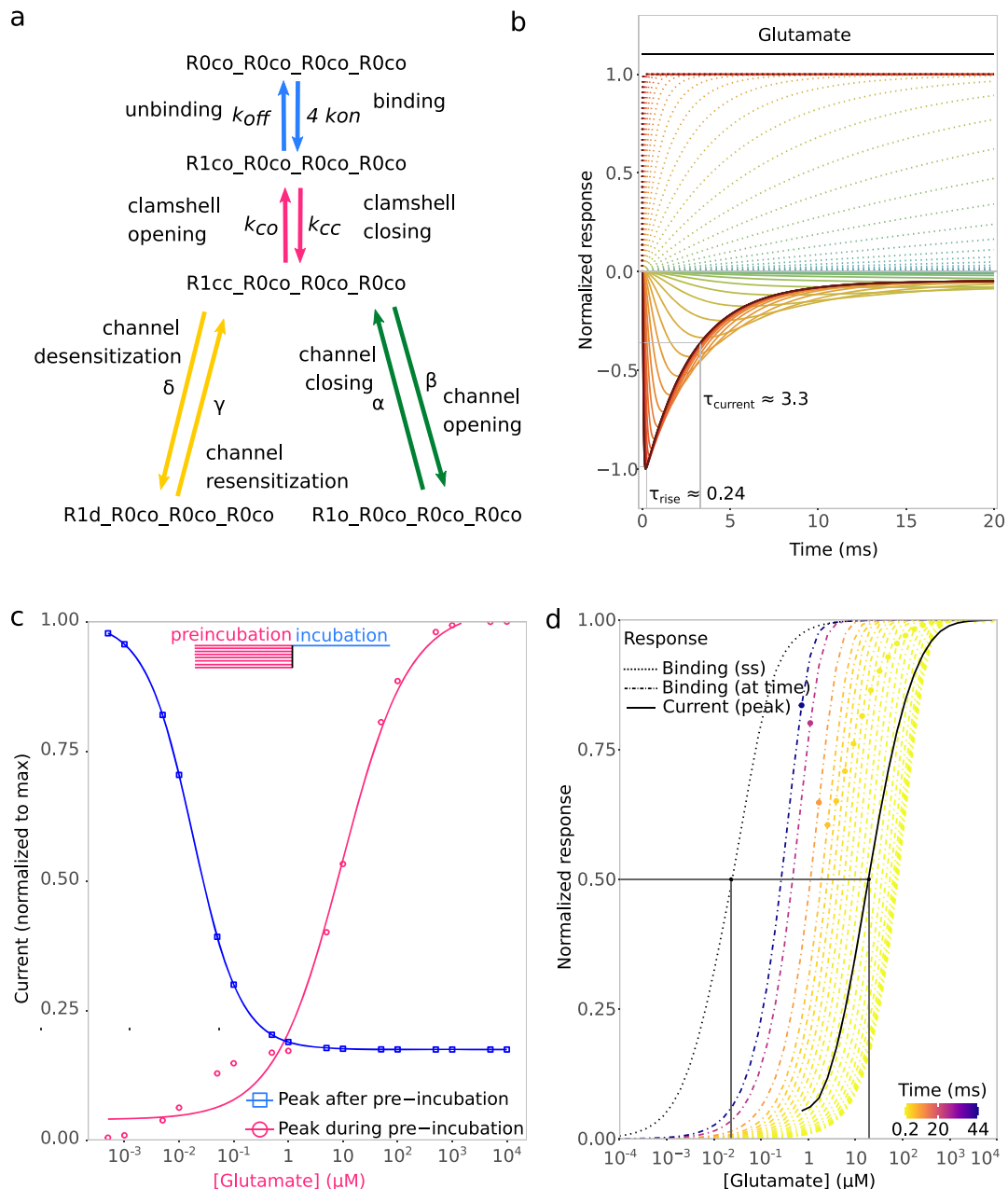
**Fig. 3 | The four-subunit model behaves qualitatively identical to the one-subunit version. a** Transitions in the four-subunit model diagram, showing only the first ligand binding event. **b** Deterministic time courses with increasing ligand concentrations. Plot shows receptor occupancy (normalized sum of all species with bound L-glutamate) and current (normalized species with at least one subunit in open configuration), drawn with negative numbers vs. time. Darker corresponds to higher ligand (L-glutamate) concentration. **c** Inset shows the design of the simulated pre-incubation experiment. Red: peak current vs L-glutamate concentration during pre-incubation. Blue: peak current obtained when stimulated with $10^4$ μM L-glutamate after being preincubated with the indicated L-glutamate concentrations. **d** Plot shows the dose–response curves for peak current (solid), steady-state ligand binding (dotted line), and ligand binding at different times after the addition of L-glutamate (coded using a colormap). Colored circles highlight binding at the time of peak current at the indicated L-glutamate concentrations. The values used for the dose–response curves are from (**b**). Ligand concentrations that elicit 50% of maximum response are marked with solid black lines for the steady-state ligand binding and peak current dose–response curves.

out which part of the channel operation was relevant, we next explored the relative role of the desensitization and resensitization ($\delta$ and $\gamma$) relative to the opening and closing ($\beta$ and $\alpha$) transition rates (Fig. 4d). We found that separation between the steady state binding and peak current dose–response curves (i.e., the highest capacity to capture pre-equilibrium information) depended on the speed of $\delta$ and $\gamma$. Note that although $\beta$ and $\alpha$ channel rates need to be faster than $\delta$ and $\gamma$ rate, otherwise no current peak occurred, their values did not control separation.

## The desensitization rate is a main controller of the position of the peak current dose–response curve

The characteristic transient current of AMPAR is caused by a rapid desensitization ($\delta$) followed by a relatively slow resensitization ($\gamma$) (800 s$^{-1}$ vs 45 s$^{-1}$), so that the channel stays desensitized for some time. The above results showed that the speed of the desensitization process is critical for PRESS. Thus, we next asked the individual role of each of these two rates. Increasing the desensitization rate shifted the current dose–response curve
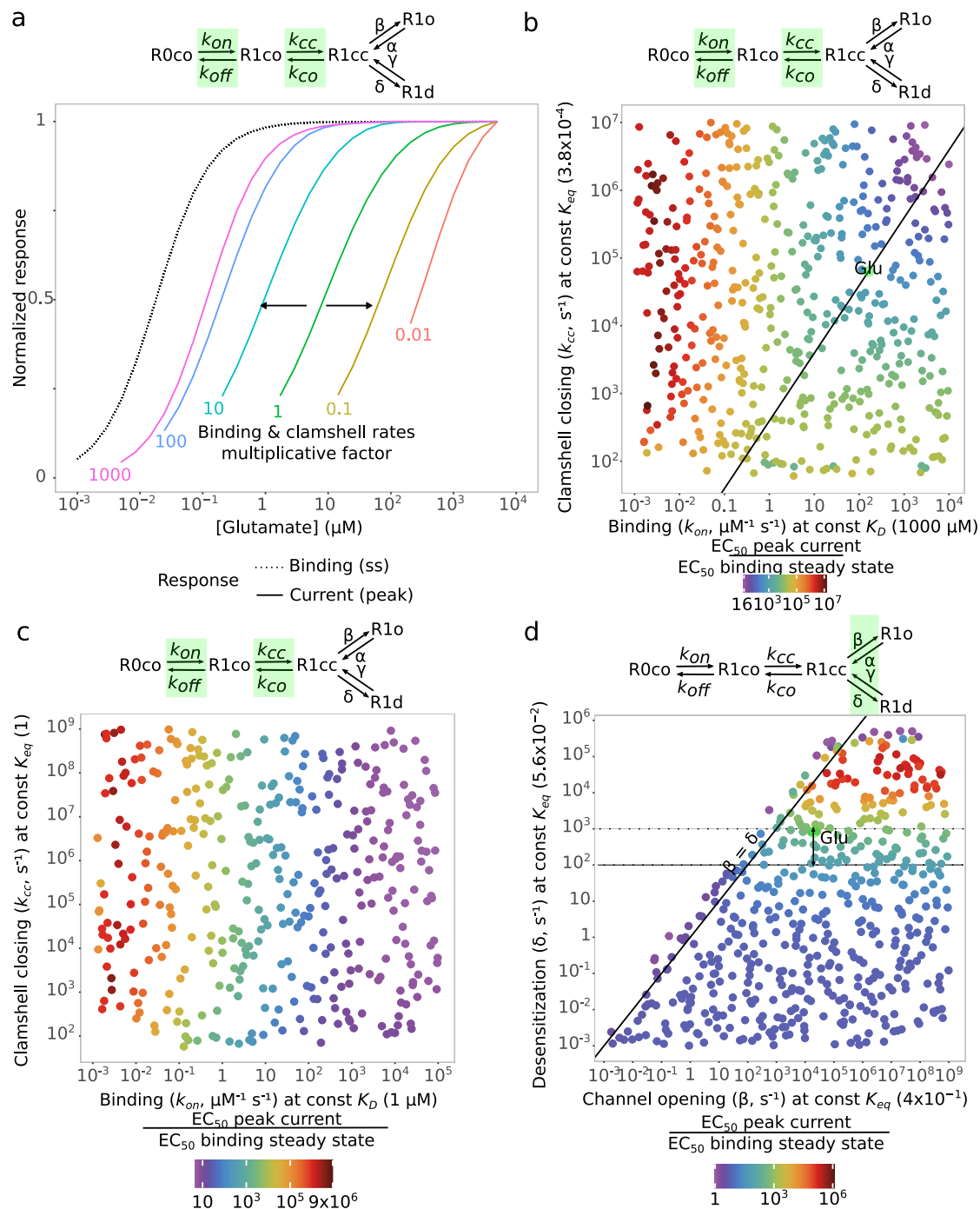
**Fig. 4 | The peak current does capture pre-equilibrium binding information.**
**a** Steady state binding and peak current dose–response curves with binding and
clamshell rates multiplied by the indicated factor. Peak current dose–response
curves in color, with experimentally measured rates (factor 1) centrally (green),
slower (yellow and red) and faster (cyan, blue, and purple) rates shifting right and
left, respectively. Inset shows the model diagram with the modified rates highlighted
in green. **b** $EC_{50}$ ratio between the steady state binding and peak current
dose–response curves for the explored binding and clamshell parameter space. Axes
show the binding ($k_{on}$) and clamshell closing ($k_{cc}$) rates, and the model is run at
constant $K_D$ ($k_{off}/k_{on}$) and $K_{eq}$ ($k_{co}/k_{cc}$). **c** $EC_{50}$ ratio between the steady state binding

and peak current dose–response curves for the explored binding and clamshell rates
with clamshell equilibrium constant ($K_{eq}$) equal to 1 and binding equilibrium
constant ($K_D$) equal to 1 µM. Axes show the binding ($k_{on}$) and clamshell closing ($k_{cc}$)
rates. **d** $EC_{50}$ ratio between the steady state binding and peak current dose–response
curves for the explored opening and desensitization parameter space. Axes show the
opening ($k_o$) and desensitization ($K_D$) rates, and the model is run at constant $K_{eq}$ ($k_o/$
$k_c$) and $K_{eq}$ ($k_r/K_D$). **b, d** "Glu" marks the location in the parameter space where
AMPAR stimulated with L-glutamate lies. **d** The arrow next to Glu indicates the
range where L-glutamate: AMPAR lies due to changes in desensitization rate caused
by subunit composition or association with accessory proteins (see Discussion).

to the right, and reducing it shifted it to the left (Fig. 5a). Also, at lower
desensitization rates, the current did not exhibit a clear peak (Fig. 5d).

Interestingly, changing the desensitization rate $\delta$ also changed the
position of the binding dose–response curve, but in the opposite direction,

so that the binding and current dose–responses separated even further upon
increasing the desensitization rate. The change in the binding curve to an
apparent higher affinity at higher desensitization rates is consistent with the
idea that increasing desensitization slows down the apparent unbinding rate
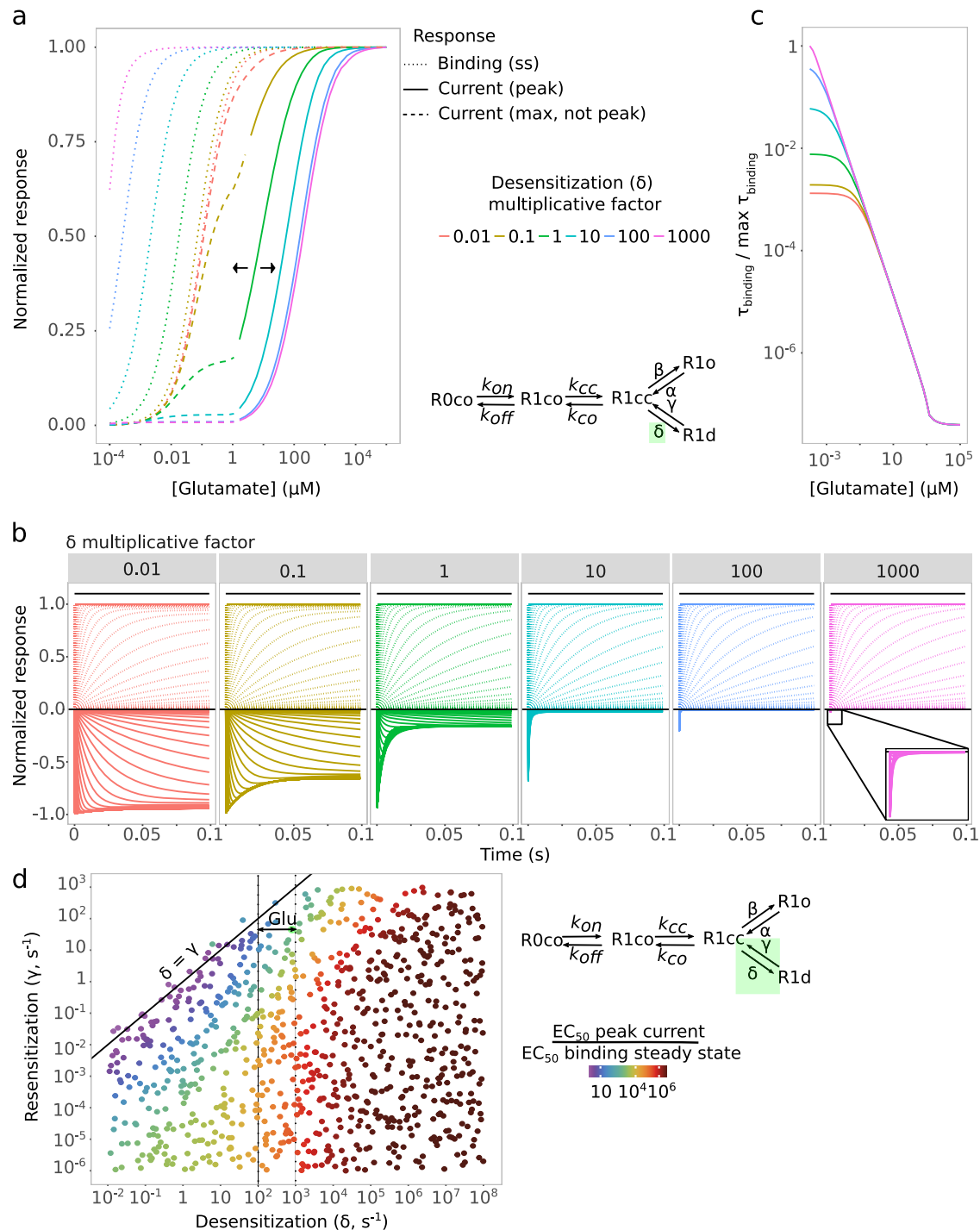
**Fig. 5 | Desensitization controls dose–response curve separation. a** Steady state binding and peak current dose–response curves with base (rates used for AMPAR so far) and factor-multiplied desensitization rates. Peak current dose–response (solid) and binding (dashed) curves in color, with experimentally measured rates centrally (green), and slower (yellow and red) and faster (cyan, blue and purple) rates shifting respectively left and right. **b** Deterministic time courses with increasing ligand concentrations for the rates in (**a**). Plot shows all binding (normalized sum of all species with bound L-glutamate) and current (normalized species R1o), drawn with negative numbers vs. Time. Inset for higher desensitization rate shows the small peak current elicited by the higher ligand concentrations. **c** Binding time constant τ ($\tau_{\text{binding}}$) with base and factor-multiplied desensitization rates, as in (**a**). The inset shows the model diagram with the modified rate highlighted in green. **d** $EC_{50}$ ratio between the steady state binding and peak current dose–response curves for the explored desensitization and resensitization rates. The inset shows the model diagram with the modified rates highlighted in green.

($k_{\text{off}}$). Indeed, $\tau_{\text{binding}}$ increased as we increased the desensitization rate, but only in the low L-glutamate concentration region (Fig. 5b), a region in which $\tau_{\text{binding}}$ is mostly dependent on $k_{\text{off}}$, not $k_{\text{on}}$. This result suggested that the desensitized state acted as a sink into which AMPARs fall quickly (at high desensitization rates), but from which it takes quite some time to return (the

resensitization rate was maintained constant). Consistently, increasing resensitization compensated for this effect to some extent (Fig. 5c). When exploring the parameter space for these two transitions, we find that it's mainly desensitization that controls both dose–response curves' separation (Fig. 5c).
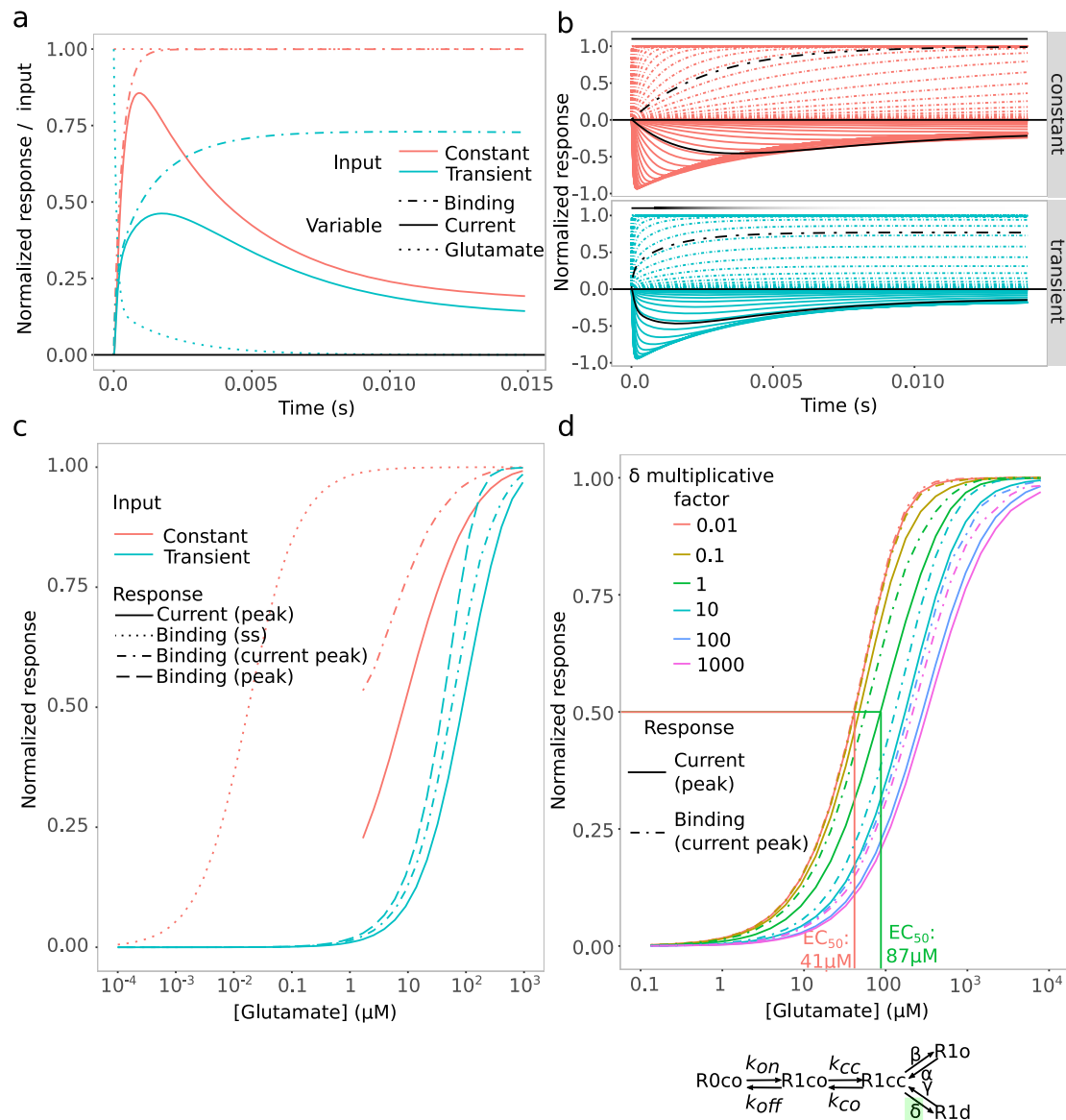
**Fig. 6 | The effect of a changing desensitization rate is diminished but not eliminated by a transient input. a** Constant and transient glutamate (double exponential decay with time constants 100 μs and 2 ms, as in Clements et al.[1]), normalized to initial maximum concentration, normalized peak current elicited by each input, and normalized bound receptors. **b** Deterministic time courses with base desensitization rate with increasing ligand concentrations for constant and transient input with decay as in (**a**), with the time course corresponding to the $EC_{50}$ concentration marked in black. Plot shows all binding (normalized sum of all species with bound L-glutamate) and current (normalized species R1o), drawn with negative numbers vs. time. **c** Peak current dose–response curves (solid) with base desensitization rate and constant (pink) or transitory (blue) ligand, steady state binding dose–response curve for constant ligand (dotted), peak binding and "binding at-current-peak" dose–response curve for transitory ligand (dashed and dash-dotted line). **d** Peak current dose–response curves with base and factor-multiplied desensitization rate. Peak current dose–response in color, with experimentally measured rates centrally (green), and slower (yellow and red) and faster (cyan, blue and purple) rates shifting respectively left and right. Inset shows the model diagram with the modified rate highlighted in green.

## A transient input also allows the use of pre-equilibrium binding information

Physiologically, the system's input is generally transient—that is, the concentration of glutamate in the synapse peaks immediately after neuro-transmitter release and then it decays rapidly, both by diffusion and because it is actively removed[4]. Thus, we wondered if PRESS could still be detected in our model in these conditions. To test that, we modeled the effect of a transient ligand by implementing a biphasic function for the disappearance of glutamate with time constants of 100 μs and 2 ms, to capture the in vivo clearance rate, as previously shown[11] (Fig. 6). As expected, in contrast to the simulations so far, bound receptor peaks after glutamate begins to decrease (Fig. 6a, b). In this case, the dose–response of peak current was shifted farther to the right with respect to that obtained with constant input, and,

notably, it nearly coincided with that of peak binding (Fig. 6c). Because binding slows when glutamate begins to disappear, and that happens before ligand-receptor binding reaction reaches equilibrium (for all but the largest glutamate concentrations simulated), we reasoned that the peak binding curve actually captured pre-equilibrium binding information. Thus, in this case, the current dose–response curve likely reflected pre-equilibrium information not only for the reasons laid out for constant input, but also because of the pre-equilibrium nature of the binding curve. If correct, then the $EC_{50}$ of the current dose–response curve should not be as dependent on the desensitization rate. This is most notable in the simulations with wild-type desensitization rates (δ multiplicative factor = 1). All parameter sets exhibit a peak current dose–response curve shifted to the right with respect to the same parameter set with a constant input (compare Figs. 6d and 5a, or

see wild type parameter set comparison in Fig. 6c), and the effect of reducing the desensitization rate is diminished (Fig. 6d). However, the 1/100 slower desensitization rate peak current $EC_{50}$ is still around half of the $EC_{50}$ obtained with the base rate (41 μM versus 87 μM), so the shift is still detectable.

## Discussion

Here, we presented a detailed kinetic analysis with well-established state models to show how AMPA receptors operate in the PRESS regime. PRESS explains why the $EC_{50}$ of glutamate measured using the amplitude of the peak current is so much larger than when measured at the binding step (current $EC_{50}$ 200–500 μM vs. apparent $K_D$ 0.5 μM). We demonstrated this by mathematical modeling using the published rates for the receptor's transitions. Both a single and a more complex four-subunit model behaved as expected from the large body of experimental work. The large separation between $K_D$ and current $EC_{50}$ is apparent in major reviews[4], but has not been studied computationally in detail. Thus, while the significant difference between AMPAR ligand affinity and the concentration required for peak current activation has long been observed, here we provide a detailed kinetic analysis demonstrating that the PRESS mechanism offers a robust explanation for this phenomenon.

AMPAR is able to work in PRESS mode because the operation of the channel itself is faster than the time it takes the ligand to reach equilibrium binding, thereby allowing the system to capture information only present before equilibrium. To demonstrate this, we simulated the model, modifying the rates of binding relative to channel operation. Of the four transitions that govern the channel, we concluded that the first two, binding and clamshell closure, combined, need to be slow (evidenced in that the rates have a multiplicative effect—i.e., it only mattered the rate of formation of the AMPAR state competent for channel opening, R1cc in the 1 subunit model) relative to channel operation, opening/closing and desensitization/resensitization. For there to be a peak current, of these two processes, opening/closing needs to be faster than desensitization/resensitization. In this way, the peak takes place some time before the ligand achieves equilibrium binding. Finally, of the desensitization/resensitization rate pair, our simulations indicated that it is the desensitization rate that controls the separation of sensing (binding) and response (current) dose–responses.

In our modeling, we have employed a desensitization rate of 800 s⁻¹. However, kinetics of AMPARs are influenced by subunit composition[12,13], naturally altering the operation of the PRESS regime. For example, homotetramers of GluA1 channels desensitize very rapidly (time constant $\tau_{current} \approx 3$–4 ms, corresponding to ~250–330 s⁻¹) while GluA2-containing receptors (especially homomeric GluA2) do so more slowly ($\tau_{current}$ on the order of 6–10 ms, ~100–170 s⁻¹). GluA3 and GluA4 subunits confer intermediate to fast gating profiles. Notably, alternative splicing at the "flip/flop" module produces further differences: for GluA2, GluA3, and GluA4, the flip isoforms desensitize significantly more slowly (longer $\tau$) than their flop counterparts. For example, flip variants of GluA2 and GluA4 have $\tau_{current} \approx 5$–6 ms, whereas the flop forms desensitize in ~1–2 ms. Indeed, GluA4(flop) is one of the fastest-desensitizing AMPARs ($\tau_{current}$ ~ 0.9 ms, >1000 s⁻¹), whereas a GluA2(flip) homomer desensitizes much more slowly ($\tau_{current}$ ~ 5.8 ms, ~170 s⁻¹). In general, GluA1-containing receptors show inherently fast desensitization (with GluA1 flip vs. flop splicing having minimal effect), whereas receptors incorporating GluA2–4 can exhibit desensitization rates spanning an order of magnitude depending on the subunit/isoform combination. Thus, the overall range of AMPAR desensitization rate constants is roughly $10^2$ s⁻¹ up to >$10^3$ s⁻¹ under saturating glutamate[12,13]. We marked this region of desensitization rates in Figs. 4d and 5d, to highlight the impact on PRESS ($EC_{50}$ peak /$EC_{50}$ss), shifting the range of concentrations where there is a concentration-dependent response to L-glutamate.

In addition, the presence of auxiliary proteins also modulates AMPAR desensitization. Transmembrane AMPAR regulatory proteins (TARPs), such as γ2 (stargazin), γ4, or γ8 generally slow entry into desensitization (2–3-fold), reducing the region of PRESS ($EC_{50}$ peak /$EC_{50}$ss closer to 1),

thereby increasing steady-state currents[14,15]. For instance, co-expression of TARP γ2 with GluA2 slows the desensitization rate from ~120 s⁻¹ to ~60 s⁻¹ [16]. Similarly, cornichon homolog auxiliary proteins (CNIH2/3) slow AMPAR desensitization in a manner akin to TARPs[14]. Cornichon-3, for example, reduces desensitization of GluA1/2 receptors from 160 s⁻¹ to 140 s⁻¹ [17]. In contrast, the accessory protein germ cell-specific gene 1-like protein (GSG1L) does the opposite, accelerating AMPAR desensitization[14,18,19], markedly increasing the region of PRESS. Thus, auxiliary subunits finely tune AMPAR desensitization kinetics: Type I TARPs (γ2, γ4, γ8) and cornichon proteins act as positive modulators that slow desensitization ($\tau_{current}$ extended into the tens of milliseconds in some complexes), whereas GSG1L acts as a unique negative modulator that accelerates desensitization and abbreviates AMPAR signaling.

The modulation on PRESS (altering receptor peak current $EC_{50}$) we described here by changing the desensitization rate ($\delta$) resembles the effect obtained by the association of the various regulators of AMPAR mentioned above. This effect of auxiliary proteins on current $EC_{50}$ is strictly dependent on the fact that AMPARs use PRESS; otherwise, these regulators would just lengthen or shorten the duration of the current pulse, without modifying the current $EC_{50}$. We speculate, then, that a potential role of TARPs and other accessory proteins is to modulate PRESS on AMPARs. Therefore, the PRESS mechanism provides a quantitative framework for interpreting the functional impact of the family of AMPAR auxiliary subunits being discovered and characterized.

On the one hand, both experiment and simulation showed that the glutamate peak ion current dose–response has an $EC_{50}$ at least in the 100 μM range. And we have shown here that the reason the current $EC_{50}$ is shifted to these higher concentrations relative to the $K_D$ (~0.5 μM) is PRESS. On the other, in the synaptic cleft AMPARs are exposed even higher glutamate concentrations (up to 1 mM[20]), suggesting that, in principle, it might not be relevant if the ion current dose–response has an $EC_{50}$ of 100 μM or 0.1 μM, as in both cases AMPARs will be equally saturated with L-glutamate. However, cells do experience a topographically-based glutamate dose–response, with maximal glutamate concentration immediately facing the site of release, diminishing steeply with distance[21,22]. That is, AMPARs further from the immediate release site will be exposed to lower concentrations. In this regard, the actual current $EC_{50}$ determines the extent of the membrane that will depolarize in response to a given neurotransmitter release. The higher the $EC_{50}$, the smaller the excitation area. Given the various shapes and receptor densities in which AMPAR is configured[6], we speculate that the current $EC_{50}$ is an important functional parameter.

In contrast to AMPARs, the glutamate N-methyl-D-aspartate receptors (NMDAR) desensitize much more slowly[4,20,23,24]. Consistent with our prediction from our models of a case with a low desensitization rate, their current $EC_{50}$ is very similar to the apparent $K_D$[4]. Thus, the same release of glutamate would activate a much larger area covered with NMDARs. However, activation of NMDARs requires an initial depolarization of the membrane, which is commonly accomplished by opening of co-localizing AMPARs[4]. Consequently, the smaller area of AMPARs activation caused by PRESS contributes to restricting the area of NMDAR activity. In addition, NMDARs participate in the major form of long-term potentiation (LTP) in the brain, the so-called NMDAR-dependent LTP. This type of LTP is thought to result from either recruitment of extra AMPARs to the membrane in the post-synapse, from an increase in the conductance of existing channels, or both[5]. Consistent with our modeling results, we suggest that modulation of PRESS via, for example, the desensitization rate through TARPs or other molecules could be one of the mechanisms of increased overall current by allowing neighboring AMPARs to activate. Characterizing AMPARs as PRESS systems now offers new insights into how spatial precision in synaptic signaling is achieved and modulated.

In our four-subunit model we assumed that each subunit behaved independently, except for the fact that the model required at least two subunits bound by ligand to be able to open the channel, and we obtained qualitatively similar results to the one-subunit model, with and even greater separation between steady-state binding $EC_{50}$ and peak current $EC_{50}$. The

assumption of independence greatly facilitates the modeling of the receptor, but it is not exactly correct, since there seems to be some degree of negative cooperativity in L-glutamate binding[25]. Although this effect is moderate, estimated at around a two-fold reduction in binding affinity, that is a small effect compared to the effect of PRESS.

Regarding the rate requirements for PRESS, modeling AMPAR showed an unexpected result. Up to now, all our results indicated that biochemical steps whose speed depended on ligand concentration (basically, binding reactions) generated dose–response curves that move to the left over time (we have called those steps, shifters), and thus enable PRESS. Because of that, the faster they operate, the shorter the time window for a downstream step to take advantage of the shift, until it is so fast that there is no possibility of PRESS. Here, we found that when a subsequent transition is slow enough (in the case of AMPAR, the transition would be clamshell closure/opening) it may compensate for an initial fast binding reaction, provided its $K_{EQ}$ of that transition is lower than 1 (as in the case of AMPAR, where clamshell closing is much faster than its opening). The interpretation of this result is that when $K_{EQ} \ll 1$, then, *ligand binding + clamshell closure* should be considered as a single step, in comparison to the slower *closure opening + ligand unbinding*.

## Methods

We developed a simple mathematical kinetic model for the AMPAR receptor using COPASI[18] that captures the essence of its behavior, based on a previously described reaction scheme that captures the main transitions of AMPARs (Fig. 2a)[9]. The model contains one state with no ligand, R0co, and four states with bound ligand, R1co, R1cc, R1o, R1d. There is one desensitized state, R1d, three closed states, R0co, R1co and R1cc, and only one open state R1o. All the transitions are reversible. We used the open-channel species (R1o) as a proxy for the current and considered all ligand-bound species for the receptor-ligand complex equilibrium.

The rates we used are listed in Table 1 and were obtained from the literature[8,10]. The model differs from some other published models in that it requires one extra conformational change after binding (closing of the clamshell-like ligand binding domain) and that open and desensitized states follow that transition in parallel and have no direct transitions. As the rates in the literature were measured at different temperatures, they were compatibilized using a temperature coefficient (Q10) of 2 for conformational changes' rates and 1.3 for the binding rates, and the models were run with rates corresponding to room temperature (22 °C). The equation used for changing the rates is (1).

$$\text{rate}_2 = \text{rate}_1 \times Q10^{\frac{\text{temp}_2 - \text{temp}_1}{10}} \qquad (1)$$

We performed steady-state and time-course simulations using the COPASI R Connector package (CoRC) with a constant input (constant ligand concentration), and time-course simulations with transient input, in which the ligand disappears as an exponential curve with two time-constants, 100 μs and 2 ms[11]. In all these simulations, all species are in solution with free diffusion, and there's no spatial modeling of the synaptic space, or postsynaptic membrane.

$$0.85 \times [\text{Glutamate}]_0 \times e^{-1000 \times \text{time}} + 0.15 \times [\text{Glutamate}]_0 \times e^{-476.19 \times \text{time}}$$
$$(2)$$

In a similar manner, we also extended the model to a more complex, four-subunit model, that presupposes independent binding and conformational transitions for all four subunits, with equal rates (see diagram in Fig. S2). Rates for transitions are multiplied by the number of subunits that can potentially undergo the transition in that step.

We used a Latin Hypercube Sampling algorithm from R package FME[26] to obtain random rates for exploring model behavior in the parameter space.

## References

1. Kim, J. Y., Borleis, J. A. & Devreotes, P. N. Switching of chemoattractant receptors programs development and morphogenesis in Dictyostelium: receptor subtypes activate common responses at different agonist concentrations. *Dev. Biol.* **197**, 117–128 (1998).
2. Ventura, A. C. et al. Utilization of extracellular information before ligand-receptor binding reaches equilibrium expands and shifts the input dynamic range. *Proc. Natl. Acad. Sci. USA* **111**, E3860-9 (2014).
3. Di-Bella, J. P., Colman-Lerner, A. & Ventura, A. C. Properties of cell signaling pathways and gene expression systems operating far from steady-state. *Sci. Rep.* **8**, 17035 (2018).
4. Traynelis, S. F. et al. Glutamate receptor ion channels: structure, regulation, and function. *Pharm. Rev.* **62**, 405–496 (2010).
5. Diering, G. H. & Huganir, R. L. The AMPA receptor code of synaptic plasticity. *Neuron* **100**, 314–329 (2018).
6. Zhang, H. & Bramham, C. R. Bidirectional dysregulation of AMPA Receptor-mediated synaptic transmission and plasticity in brain disorders. *Front. Synaptic Neurosci.* **12**, 26 (2020).
7. Greger, I. H., Watson, J. F. & Cull-Candy, S. G. Structural and functional architecture of AMPA-type glutamate receptors and their auxiliary proteins. *Neuron* **94**, 713–730 (2017).
8. Abele, R., Keinänen, K. & Madden, D. R. Agonist-induced isomerization in a glutamate receptor ligand-binding domain A kinetic and mutagenetic analysis. *J. Biol. Chem.* **275**, 21355–21363 (2000).
9. Robert, A., Armstrong, N., Gouaux, E. J. & Howe, J. R. AMPA receptor binding cleft mutations that alter affinity, efficacy, and recovery from desensitization. *J. Neurosci.* **25**, 3752–3762 (2005).
10. Robert, A. & Howe, J. R. How AMPA receptor desensitization depends on receptor occupancy. *J. Neurosci.* **23**, 847–858 (2003).
11. Clements, J. D. Transmitter timecourse in the synaptic cleft: its role in central synaptic function. *Trends Neurosci.* **19**, 163–171 (1996).
12. Quirk, J. C., Siuda, E. R. & Nisenbaum, E. S. Molecular determinants responsible for differences in desensitization kinetics of AMPA receptor splice variants. *J. Neurosci.* **24**, 11416–11420 (2004).
13. Larsen, A. H., Perozzo, A. M., Biggin, P. C., Bowie, D. & Kastrup, J. S. Recovery from desensitization in GluA2 AMPA receptors is affected by a single mutation in the N-terminal domain interface. *J. Biol. Chem.* **300**, 105717 (2024).
14. Gu, X. et al. GSG1L suppresses AMPA receptor-mediated synaptic transmission and uniquely modulates AMPA receptor kinetics in hippocampal neurons. *Nat. Commun.* **7**, 10873 (2016).
15. Coombs, I. D., MacLean, D. M., Jayaraman, V., Farrant, M. & Cull-Candy, S. G. Dual effects of TARP γ-2 on glutamate efficacy can account for AMPA receptor autoinactivation. *Cell Rep.* **20**, 1123–1135 (2017).
16. Riva, I., Eibl, C., Volkmer, R., Carbone, A. L. & Plested, A. J. R. Control of AMPA receptor activity by the extracellular loops of auxiliary proteins. *eLife* **6**, e28680 (2017).
17. Coombs, I. D. et al. Cornichons modify channel properties of recombinant and glial AMPA receptors. *J. Neurosci.* **32**, 9796–9804 (2012).
18. McGee, T. P., Bats, C., Farrant, M. & Cull-Candy, S. G. Auxiliary subunit GSG1L acts to suppress calcium-permeable AMPA receptor function. *J. Neurosci.* **35**, 16171–16179 (2015).

19. Perozzo, A. M. et al. GSG1L-containing AMPA receptor complexes are defined by their spatiotemporal expression, native interactome and allosteric sites. *Nat. Commun.* **14**, 6799 (2023).
20. Clements, J. D., Lester, R. A., Tong, G., Jahr, C. E. & Westbrook, G. L. The time course of glutamate in the synaptic cleft. *Science* **258**, 1498–1501 (1992).
21. Borgdorff, A. J. & Choquet, D. Regulation of AMPA receptor lateral movements. *Nature* **417**, 649–653 (2002).
22. Raghavachari, S. & Lisman, J. E. Properties of quantal transmission at CA1 synapses. *J. Neurophysiol.* **92**, 2456–2467 (2004).
23. Patneau, D. K. & Mayer, M. L. Structure-activity relationships for amino acid transmitter candidates acting at N-methyl-D-aspartate and quisqualate receptors. *J. Neurosci.* **10**, 2385–2399 (1990).
24. Clements, J. D. & Westbrook, G. L. Activation kinetics reveal the number of glutamate and glycine binding sites on the N-methyl-D-aspartate receptor. *Neuron* **7**, 605–613 (1991).
25. Clements, J. D., Feltz, A., Sahara, Y. & Westbrook, G. L. Activation kinetics of AMPA receptor channels reveal the number of functional agonist binding sites. *J. Neurosci.* **18**, 119–127 (1998).
26. Soetaert, K. et al. Solving differential equations in R. *AIP Conf. Proc.* **1281**, 31–34 (2010).

## Author contributions
H.B. performed the simulations. H.B., A.C.V., and A.C.L. analyzed the results. A.C.V. and A.C.L. conceived the project. H.B., A.C.V., and A.C.L. wrote the paper. All authors reviewed the manuscript.

## Competing interests
The authors declare no competing interests.

## Additional information

**Supplementary information** The online version contains supplementary material available at https://doi.org/10.1038/s41540-025-00546-6.

**Correspondence** and requests for materials should be addressed to Alejandra C. Ventura or Alejandro Colman-Lerner.

**Reprints and permissions information** is available at http://www.nature.com/reprints

**Publisher's note** Springer Nature remains neutral with regard to jurisdictional claims in published maps and institutional affiliations.